1 March 2001

ELSEVIER

Optics Communications 189 (2001) 15–19

OPTICS COMMUNICATIONS

www.elsevier.com/locate/optcom

Synthesis of filters for specified axial irradiance by use of phase–space tomography

Walter D. Furlan [a,*], Dobryna Zalvidea [b], Genaro Saavedra [a]

[a] *Departamento de Óptica, Universitat de València, c/o Dr. Moliner 50, E-46100 Burjassot, Spain*
[b] *Centro de Investigaciones Ópticas, P.O. Box 124, 1900 La Plata, Argentina*

Received 6 September 2000; received in revised form 9 January 2001; accepted 10 January 2001

Abstract

A procedure for designing pupil filters for applications where specified axial responses are required is developed. The method is based on the mathematical relationship between the axial impulse response of a system and the Wigner distribution function (WDF) associated to its pupil function. The desired axial irradiance, which can also have a predefined behavior depending on spherical aberration, is used to obtain this WDF by tomographic reconstruction. The synthetic pupil is retrieved from this distribution. © 2001 Published by Elsevier Science B.V.

Keywords: Axial irradiance; Pupil synthesis; Phase–space tomography; Wigner distribution function

1. Introduction

The control of the axial impulse response provided by optical systems is a matter of interest in many applications as, for example, those in which either extended depth of focus or axial superresolution is needed. Several techniques have been recently used to design pupil masks for achieving such particular features [1,2]. However, in most of these techniques optical aberrations are not taken into account. For most real systems the influence of optical aberrations on the axial irradiance must be reduced, but there are particular cases in which certain amount of aberration is desirable, for example, to obtain a larger maximum axial intensity than in the aberration-free case [3]. Therefore, the synthesis of pupil masks for specified axial irradiance distribution which also keep control over aberrations have a wide range of potential applications. Motivated by this idea, in this work we propose a novel pupil synthesis procedure to generate any wanted axial irradiance distribution with a spherically aberrated system. The method is based on the mathematical relationship between a phase–space representation of the pupil function and the axial irradiance response provided by the system [4]. The required pupil mask is obtained through a tomographic reconstruction in the phase–space domain.

2. Basic theory

Let us start by considering the irradiance impulse response, computed under the Fresnel–Kirchhoff approximation, provided by an aberrated

* Corresponding author. Fax: +34-963-864-715.
E-mail address: walter.furlan@uv.es (W.D. Furlan).

0030-4018/01/$ - see front matter © 2001 Published by Elsevier Science B.V.
PII: S0030-4018(01)01027-6

optical imaging system [5]. It is straightforward to show that, for axial points and a spherically aberrated system, this response is given by [4]

$$I(\omega_{20};\omega_{40}) = \left| \frac{1}{\lambda f(f+z)} \int_0^{2\pi} \int_0^a t(r,\theta) \times \exp\left[i\frac{2\pi}{\lambda}\omega_{40}\left(\frac{r}{a}\right)^4 \right] \times \exp\left[i\frac{2\pi}{\lambda}\omega_{20}\left(\frac{r}{a}\right)^2 \right] r\,dr\,d\theta \right|^2, \tag{1}$$

$t(r,\theta)$ being the pupil function of the system expressed in polar coordinates. In Eq. (1), ω_{40} denotes the coefficient for Seidel's spherical aberration, and z is the axial coordinate as measured from the paraxial image plane, located at a distance f from the pupil. These distances are related to the maximum extent a of the pupil function through the defocus coefficient ω_{20} defined as

$$\omega_{20} = \frac{-za^2}{2f(f+z)}. \tag{2}$$

In this way, the left-hand side of Eq. (1) can be understood as a function of the axial distance z by substituting the parameter ω_{20} from Eq. (2).

In Ref. [4] it has been shown that, for large Fresnel numbers, the set of axial irradiances given by Eq. (1) can be expressed as

$$I(\omega_{20};\omega_{40}) = \int_{-\infty}^{\infty} W_q\left(x, \frac{-2\omega_{40}}{\lambda}x - \frac{\omega_{20}+\omega_{40}}{\lambda}\right) dx, \tag{3}$$

being

$$W_q(\xi,\nu) = \int_{-\infty}^{\infty} q(\xi+\xi'/2)q^*(\xi-\xi'/2) \times \exp(i2\pi\nu\xi')\,d\xi' \tag{4}$$

the bidimensional (2-D) Wigner distribution function (WDF) of a modified pupil function

$$q(\zeta) = t_0(r) = \frac{1}{2\pi}\int_0^{2\pi} t(r,\theta)\,d\theta, \tag{5}$$

where the variable ζ is defined as

$$\zeta = \left(\frac{r}{a}\right)^2 - 0.5. \tag{6}$$

Eq. (3) shows that the axial behavior of the irradiance distribution provided by a system with an arbitrary value of spherical aberration – ω_{40} is a parameter in this equation – can be obtained from a single WDF of the mapped pupil $q(\zeta)$ of the system, by integrating the values of this function along straight lines in the phase–space domain. The slope, $m = -2\omega_{40}/\lambda$, and the y-intersect, $\nu_0 = -(\omega_{20}+\omega_{40})/\lambda$, of these lines are given by the spherical aberration and defocus coefficients.

For our purposes we can take advantage of this representation by recognizing that the line integral in Eq. (3) for all values of ω_{20} and ω_{40} is actually the Radon transform of the above WDF, or the Radon–Wigner transform (RWT) of the function $q(\zeta)$ [6]. In fact, by use of the geometry shown in Fig. 1, this RWT may be considered as the projection of $W_q(x,\nu)$ onto an axis x' rotated an angle ϕ with respect to the x axis [7]. In mathematical terms

$$\Re[W_q(x,\nu);x',\phi] = \int_{-\infty}^{\infty} W_q(x'\cos\phi - \nu' \times \sin\phi, x'\sin\phi + \nu'\cos\phi)\,d\nu' = \int_{-\infty}^{\infty} W_q\left(x, -\tan^{-1}\phi + \frac{x'}{\sin\phi}\right) dx, \tag{7}$$

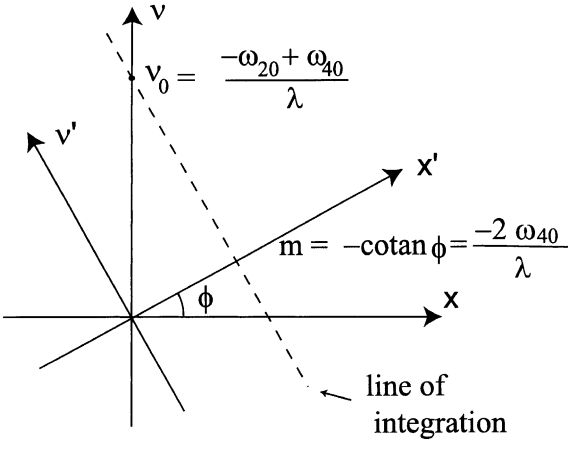

Fig. 1. Phase–space coordinates for the Radon transform of the WDF.

where $\mathfrak{R}$ is an operator representing a Radon transform. Therefore it is straightforward to show that Eq. (3) can be written as

$$I(\omega_{20};\omega_{40}) = \mathfrak{R}[W_q(x,v);x',\phi], \tag{8}$$

where

$$\phi = \tan^{-1}\left(\frac{\lambda}{2\omega_{40}}\right), \qquad x' = -\frac{\omega_{20}+\omega_{40}}{\sqrt{4\omega_{40}^2+\lambda^2}}\ . \tag{9}$$

Eq. (8) is the keystone of our design method. In fact, the synthesis procedure starts by taking notice that this equation can be inverted to obtain the 2-D WDF by means of the inverse Radon transform. In this way, we can perform a tomographic reconstruction of W_q from the projected function $I(\omega_{20};\omega_{40})$, representing the irradiance at the axial points – variable ω_{20} – for a sufficient set of values of ω_{40}.

There are several forms of the inverse Radon transform. Their common basis is the central-slice theorem, which, applied to our case, states that the one-dimensional (1-D) Fourier transform of the projection $I(\omega_{20};\omega_{40})$ – the Radon transform – and one line of the 2-D Fourier transform of $W_q(x,v)$ are mathematically identical. This line corresponds to the v' axis of the rotated phase–space coordinates (see Fig. 1) defined by the value of the spherical aberration coefficient. Thus, the entire 2-D Wigner space can be sampled on a set of lines defined by the parameters ω_{20} and ω_{40}. The implementation of the inverse Radon transform makes use of the filtered back-projection algorithm [8]. The back-projection operation converts a 1-D function – the axial irradiance for a fixed value of ω_{40}, in our case – into a 2-D function by smearing it uniformly along the original projection direction – defined by the v' axis in Fig. 1. Then the algorithm calculates the summation function which results when all back-projections are summed over all projection angles ϕ i.e., different values of ω_{40}. The final reconstructed function $W_q(x,v)$ is obtained by a proper filtering of the summation image [8].

Once the WDF is synthesized with the values of the input axial irradiances, the pupil function is obtained by inverting the WDF in Eq. (4) as follows

$$q(\zeta) = \frac{1}{q^*(0)}\int_{-\infty}^{\infty} W_q(x,\zeta/2)\exp(-\mathrm{i}2\pi x\zeta)\,\mathrm{d}x. \tag{10}$$

As a final step, the geometrical mapping in Eq. (6) is inverted to provide $t_0(r) = q(\zeta)$. Note that the recovered pupil function is actually the angular average of a more general pupil $t(r,\theta)$, i.e $t_0(r) = t(r,\theta)$ only if $t(r,\theta)$ is rotationally symmetric. This fact can be considered as another degree of freedom of our synthesis procedure, in such a way that to obtain a predefined axial behavior the designer can choose between several functions $t(r,\theta)$ having the same angular average $t_0(r)$.

3. Examples

In order to illustrate the method we have numerically simulated two examples. In the first one we tested our proposal with the synthesis of an annular apodizer that has been extensively studied [9–11]

$$t_0(r) = \frac{\operatorname{sinc}\left\{2\left[\left(\frac{r}{a}\right)^2-0.5\right]\right\} - \cos\left\{2\pi\left[\left(\frac{r}{a}\right)^2-0.5\right]\right\}}{\left\{2\pi\left[\left(\frac{r}{a}\right)^2-0.5\right]\right\}^2} \times \operatorname{circ}\left(\frac{r}{a}\right). \tag{11}$$

Fig. 2a pictures a profile of this pupil function. It has been shown that its main features are to increase the focal depth and also to reduce the influence of spherical aberration. From this function we numerically determined, first the W_q function using the WDF definition in Eq. (4), and thereby the projected distributions defined in Eq. (3), obtaining the axial irradiance distribution for different values of spherical aberration. In this case we used 1024 values for both ω_{40}/λ and ω_{20}/λ, ranging from -16 to $+16$. We treated this distributions as if they represented the desired axial behavior for a variable spherical aberration, and we reconstructed the WDF using a standard filtered back-projection algorithm for the inverse Radon transform [7,8]. From the reconstructed WDF we obtained the synthesized pupil function

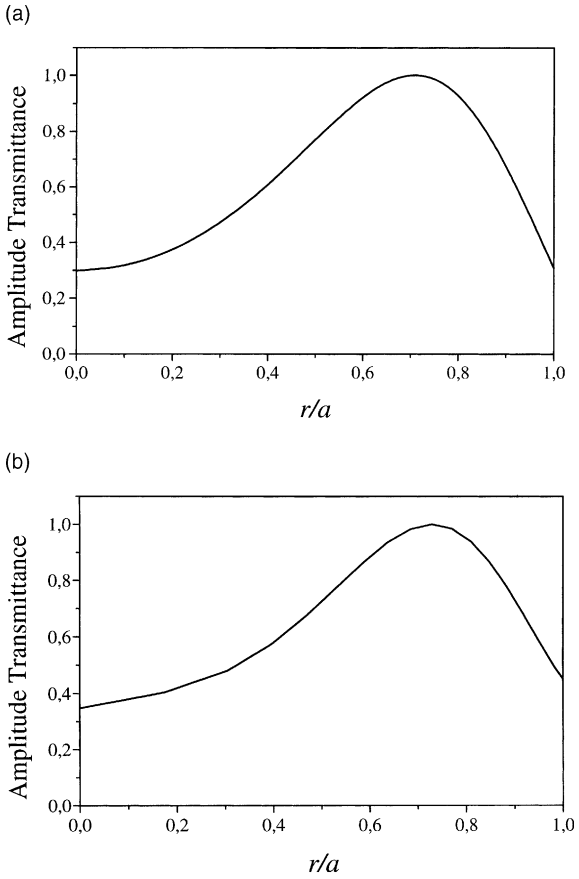

Fig. 2. (a) Amplitude transmittance of the pupil represented by Eq. (11) as a function of the normalized radial coordinate. (b) Phase–space tomographic reconstruction of the same pupil.

$t_0(r)$ by performing the discrete 1-D inverse Fourier transform of W_q in Eq. (10). The result is shown in Fig. 2b. As can be seen the amplitude transmittance of the synthesized pupil function closely resembles the original apodizer in Fig. 2a.

In a second example we considered the more interesting situation. We start by selecting a set of axial irradiances and then calculating the required pupil function. Our intention was to design a pupil mask with high sensitivity to spherical aberration on the axial irradiance. That is to say a pupil that will produce a constant intensity profile for different defocus coefficients in a certain range, but only for a single value of the spherical aberration coefficient. Fig. 3 shows the result obtained with

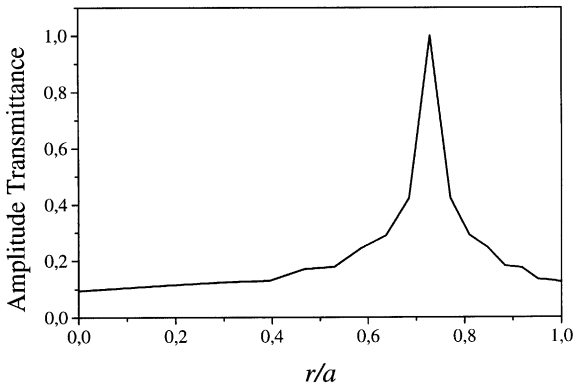

Fig. 3. Amplitude transmittance of the synthesized pupil function obtained for a high sensitivity to the spherical aberration and providing a constant axial-intensity profile.

the same sampling of the aberration functions as in Fig. 2. In this case we considered zero-intensity values for ω_{40}/λ out of the range $-0.025 < \omega_{40}/\lambda < 0.025$. In order to evaluate this last result, the synthesized pupil can be compared favorably with the annular pupils obtained for focusing applications in Ref. [1]. In fact in this reference the employed synthesis methods did not allow the use of the spherical aberration as a free parameter. However, as those examples were computed for $\omega_{40} = 0$ and in our case $I(\omega_{20}; \omega_{40}) = 0$ except for a small range of ω_{40}, both results are qualitatively comparable.

4. Conclusions

We have presented a novel method to design pupil masks that are able to generate arbitrary predefined axial irradiances. The method is based on the tomographic reconstruction of the WDF associated to the pupil. Besides the novelty in its conception, the main feature of the method is the fact that the designer can program the axial irradiance to hold a predefined behavior for different values of spherical aberration. Two examples have been presented: the first one to validate the method, and the second one to show how to design a pupil for a system with high sensitivity to the spherical aberration but producing a constant intensity-axial profile.

Further work is currently being done to improve the efficiency of the practical numerical implementation of the technique here proposed. For instance, the mathematical symmetries exhibited by the WDF can be used to decrease the number of samplings needed for its accurate tomographic reconstruction. As a result, a noticeable drop in the required computation time is expected.

Additionally, as is well known, the RWT of a function is closely related to the magnitude squared of its fractional Fourier transform (FrFT) [12]. Consequently, the left-hand side of Eq. (8) equals the magnitude square of the FrFT of order determined by the parameters ω_{20} and ω_{40}. Therefore, some properties of the FrFT could be conveniently exploited in this context.

Acknowledgements

This work was supported by the project GV99-100-1-01 of the Conselleria de Cultura, Educació i Ciència de la Generalitat Valenciana (Spain). The authors would like to thank Dr. Enrique Silvestre for his programming assistance and to an anonymous referee for his/her valuable comments.

References

[1] C.J.R. Sheppard, J. Mod. Opt. 43 (1996) 525.
[2] M. Martínez-Corral, P. Andrés, C. Zapata-Rodríguez, M. Kowalczyk, Opt. Commun. 165 (1999) 267.
[3] D. Jiang, J. Stamnes, Pure Appl. Opt. 6 (1997) 85.
[4] G. Saavedra, W.D. Furlan, E. Silvestre, E.E. Sicre, Opt. Commun. 139 (1997) 11.
[5] J.W. Goodman, Introduction to Fourier Optics, McGraw-Hill, New York, 1996 (Chapter 6).
[6] J.C. Wood, D.T. Barry, IEEE T. Signal Process. 42 (1994) 2094.
[7] G.T. Herman, Image Reconstruction from Projections, Academic Press, New York, 1980.
[8] H.H. Barret, Prog. Opt. 21 (1984) 217.
[9] J. Ojeda-Castañeda, L. Berriel-Valdós, E. Montes, Opt. Lett. 8 (1983) 458.
[10] J. Ojeda-Castañeda, P. Andrés, A. Díaz, Opt. Lett. 11 (1986) 487.
[11] J. Ojeda-Castañeda, P. Andrés, A. Díaz, J. Opt. Soc. Am. A 5 (1988) 1233.
[12] H.M. Ozaktas, B. Barshan, D. Mendlovic, L. Onural, J. Opt. Soc. Am. A 11 (1994) 547.